Applied Catalysis B: Environmental 84 (2008) 223–232

Contents lists available at ScienceDirect

Applied Catalysis B: Environmental

journal homepage: www.elsevier.com/locate/apcatb

Zirconia-supported bimetallic RhPt catalysts: Characterization and testing in autothermal reforming of simulated gasoline

Reetta K. Kaila [a,*], Andrea Gutiérrez [a], Riku Slioor [a], Marianna Kemell [b], Markku Leskelä [b], A. Outi I. Krause [a]

[a] Helsinki University of Technology (TKK), Department of Biotechnology and Chemical Technology, P.O. Box 6100, FI-02015 TKK, Finland
[b] University of Helsinki, Laboratory of Inorganic Chemistry, P.O. Box 55, FI-00014, University of Helsinki, Finland

ARTICLE INFO

Article history:
Received 29 January 2008
Received in revised form 28 March 2008
Accepted 5 April 2008
Available online 11 April 2008

Keywords:
Hydrogen
Solid oxide fuel cell
Autothermal reforming
Simulated gasoline
Bimetallic
Zirconia
Rh-Pt-O ternary system
Rh_xPt_{1-x} alloy
Rh_2O_3
Characterization

ABSTRACT

The behavior of ZrO_2-supported RhPt catalysts was studied in the autothermal reforming of simulated gasoline to produce fuel gas (H_2, CO, CO_2, CH_4, and H_2O) suitable for solid oxide fuel cell applications.

The bimetallic catalysts were superior to the monometallic Rh and Pt catalysts, and only a small addition of Rh increased the activity of the Pt catalyst markedly. Moreover, the reforming selectivity and the stability of bimetallic RhPt catalysts against carbon deposition improved with increasing Rh/Pt molar ratio.

Strong synergism between Rh and Pt was observed, leading to excellent catalytic performance. Based on TPR-, SEM-, and EDX-results a Rh-Pt-O ternary system with Rh_xPt_{1-x}–Rh_2O_3 equilibrium is suggested for the bimetallic catalysts, where Rh_2O_3 is the active site.

1. Introduction

For energy production, substitution of fossil fuels by H_2 is a suitable option for reducing the greenhouse gas emissions to the atmosphere, in particular CO_2. The major advantages of using H_2 or H_2-rich mixtures, i.e. syngas, as fuel include the diversity of primary fuels (natural gas, biomass, crude oil) that can be used in H_2 production, its clean combustion and the possibility of long-term storage of the primary fuel [1,2]. The growing interest in fuel cell technologies in heat and power production and as replacements for internal combustion engines increases the demand for H_2 production [3]. The development of an economy based on H_2 requires major structural changes that could take several decades. Therefore, commercially available fuels such as gasoline and diesel could be used as near- and mid term H_2 carriers to achieve some immediate reduction in green house gas emissions [1].

H_2-rich mixtures are industrially produced by steam reforming (SR, Eq. (1)) of natural gas on Ni catalysts [4–6]. One of the major problems encountered with this process is catalyst deactivation due to carbon deposition (Eqs. (2)–(4)).

$$C_xH_y + xH_2O \Leftrightarrow \left(\frac{y}{2} + x\right)H_2 + xCO \quad \text{(SR)} \tag{1}$$

$$C_xH_y \Leftrightarrow mH_2 + C_{x-m}H_{y-2m} + mC_{(s)} \tag{2}$$

$$2CO \Leftrightarrow CO_2 + C_{(s)} \quad \text{(Boudouard reaction)} \tag{3}$$

$$CO + H_2 \Leftrightarrow H_2O + C_{(s)} \tag{4}$$

The reforming of higher hydrocarbons (gasoline and diesel), which contain aromatics, increases the risk of carbon deposition, especially on a Ni catalyst [5]. With higher hydrocarbons, moreover, the SR becomes very endothermic, thus the combination of SR and partial oxidation (POX, Eq. (5)), known as autothermal reforming (ATR), is preferred. The hydrocarbons react with H_2O and O_2 in a process where high energy efficiencies are achieved as the exothermic POX reaction provides the heat needed for the endothermic SR reaction. The process is simple in design and requires low monetary investments [7]. The water gas shift reaction (WGS, Eq. (6)) also takes place and the reaction

* Corresponding author. Tel.: +358 9 451 2666; fax: +358 9 451 2622.
E-mail address: reetta.kaila@tkk.fi (R.K. Kaila).

0926-3373/$ – see front matter © 2008 Elsevier B.V. All rights reserved.
doi:10.1016/j.apcatb.2008.04.001

equilibrium can be shifted with changes in operating conditions: the steam to carbon and the oxygen to carbon molar ratios and the temperature. By optimizing the reforming conditions, moreover, the carbon deposition can be limited [1,2,6].

$$C_xH_y + \tfrac{x}{2}O_2 \Leftrightarrow \tfrac{y}{2}H_2 + xCO \quad (POX) \tag{5}$$

$$H_2O + CO \Leftrightarrow H_2 + CO_2 \quad (WGS) \tag{6}$$

The conventional Ni-based catalysts are also very sensitive for sulfur present in commercial fuels. This limitation can be overcome by the addition of a second metal to the Ni catalyst such as Pt or Pd [8], or the substitution of Ni by these more sulfur-resistant noble metals [6,9]. Rh in particular has shown high resistance to carbon deposition and sulfur poisoning, yielding high conversions of hydrocarbons and high selectivity for H_2 [3,10,11]. The material used as the support also affects the catalyst performance [8]. Zirconia (ZrO_2) is the preferred support for Rh catalysts in order to avoid the detrimental interaction between Rh and alumina (Al_2O_3) that reduces the activity of the catalyst [12]. As ZrO_2 is less acidic than Al_2O_3 [13], thermal cracking reactions and coke formation are reduced [14]. The disadvantage of ZrO_2 is, however, the low surface area compared to other supports [12].

Previously, we presented results on ATR of *n*-dodecane, toluene, and their mixture on ZrO_2-supported noble metal catalysts [15]. The Rh catalyst became deactivated with time on stream. We proposed that the catalyst deactivation was caused by the formation of volatile Rh compounds that vaporized from the catalyst surface at high temperatures, in accordance with the results presented by Bagot et al. [16]. They reported that the presence of free oxygen atoms drives segregation on Pt-Rh surfaces, causing vertical diffusion of Rh from the second atomic layer to the surface layer [16]. Furthermore, the topmost, Rh-enriched surface appears unstable beyond 300 °C, and dramatic Rh depletion is observed [16], especially if the oxidation of Rh is rapid [17]. However, the thermal stability of the catalyst was improved when Rh was combined with Pt to form a bimetallic catalyst [15].

Bimetallic RhPt catalysts play a crucial role in simultaneous oxidation of hydrocarbons and CO, and reduction of NO_x from automobile exhaust gases. Extensive research has, thus, been carried out on these three-way catalysts [16,18–21]. However, the behavior of RhPt catalysts has mainly been studied on a theoretical level, using flat, single crystal metal samples [18,20,22,23], where the presence of a Rh_xPt_{1-x} alloy is considered a certainty [18]. Indeed, bimetallic RhPt catalysts have been superior to monometallic catalysts, suggesting synergism between the two metals [24,25] and the formation of an alloy [26,27].

In this work, ZrO_2-supported mono- and bimetallic RhPt catalysts, with various Rh/(Rh + Pt) ratios, were characterized and tested in ATR reactions of simulated gasoline to better understand the roles of Rh and Pt on the bimetallic catalysts. The synergism between Rh and Pt on the ZrO_2-supported catalysts is discussed and the presence of a ternary Rh-Pt-O system and a Rh_xPt_{1-x}–Rh_2O_3 equilibrium in an oxidizing environment [17] is considered.

2. Experimental conditions

2.1. Catalyst preparation

The mono- and bimetallic catalysts were prepared by dry impregnation and dry co-impregnation, respectively, using $Pt(NH_3)_2(NO_2)_2$ (Aldrich, 3.4 wt% in dilute ammonium hydroxide), $Rh(NO_3)_3$ (Aldrich, 10 wt% Rh in >5 wt% nitric acid), and their solutions. The intended total metal loading on the surface of both mono- and bimetallic catalysts was 0.5–1.0 wt%. The ZrO_2 support (MEL Chemicals EC0100) was ground to a particle size of 0.25–0.42 mm and calcined at 900 °C for 16 h (temperature ramp 5 °C/min). After impregnation, the catalysts were dried at room temperature for 4 h and at 100 °C overnight. Finally the catalysts were calcined at 700 or 900 °C for 1 h (temperature ramp 1.3 °C/min).

The mono- and bimetallic catalysts were designated Pt, 0.5RhPt, 1RhPt, 2RhPt, and Rh, where the numbers 0.5, 1, and 2 correspond to the intended Rh/Pt molar ratio of the bimetallic catalysts, respectively. The calcination temperature is indicated in parentheses: (700) or (900).

2.2. Catalyst characterization

Metal loadings of the fresh and used catalysts were analyzed by inductively coupled plasma-atomic emission spectroscopy (ICP-AES, Varian-Liberty). The analytical error of this procedure is ±5%. For comparative purpose, the metal loadings of the fresh catalysts were measured with a X-ray fluorescence spectrometer (Philips PW 1480 XRF) equipped with UniQuant 4–software.

BET-surface area and total pore volume determinations were performed with a Coulter Omnisorp 100 CX gas adsorption instrument using static volumetric adsorption and desorption method, where N_2 (Aga, 99.999%) was used as an adsorptive gas. The measurements were done for an evacuated catalyst sample (0.1 g) in a liquid-N_2 bath at 77 K (−196 °C). The adsorption isotherm was measured by dosing N_2 to the sample and measuring the adsorbed amount as a function of N_2 pressure. The H_2 (Aga, 99.999%) chemisorption determination was performed with the same equipment in pulses of H_2 (15 steps) and the experimental setup is reported in detail elsewhere [15]. The analytical error of these procedures is ±10%.

CO (Messer Griesheim, 99.997%) adsorption was studied by *in situ* diffuse reflectance Fourier transform infrared spectroscopy (DRIFTS) as reported previously [15]. The experimental setup is described in detail elsewhere [28].

Temperature programmed reduction (TPR) with H_2 (Aga, 99.999%) was carried out by Altamira Instruments AMI-100 characterization equipment. The catalyst samples (80 mg) were flushed with Ar (Aga, 99.999%), heated from 30 to 160 °C at a rate of 10 °C/min, and held at 160 °C for 30 min. Subsequently, the samples were heated from 160 to 700 °C at a rate of 15 °C/min under a flow of 20% O_2/He (Aga, 99.996%) and kept at 700 °C for 60 min. The samples were cooled to 50 °C in 20% O_2/He flow. TPR was performed at a heating rate of 10 °C/min up to 700 °C under a flow (30 cm^3/min, NTP) of 5% H_2/Ar (Aga, 99.999%). The consumption of H_2 was monitored by a thermal conductivity detector (TCD).

The X-ray diffraction (XRD) measurements were performed with a Philips PW 1710 and X-ray photoelectron spectroscopy (XPS) determinations were performed with AXIS 165 by Kratos Analytical.

Scanning electron microscopy (SEM) was performed with a LEO 1450 SEM (Oxford Instruments Inca). Secondary electron and back scattered secondary electron detectors were used to record images at several magnifications.

The energy dispersive X-ray (EDX) measurements were done with an Oxford INCA 350 energy dispersive X-ray spectrometer connected to a Hitachi S-4800 field emission scanning electron microscope.

2.3. Testing in autothermal reforming

A mixture of C_7-hydrocarbons was prepared to simulate commercial gasoline. The approximate composition of gasoline

varies widely depending on the source and the blending of different refinery streams. In this C_7-mixture, toluene (T, Riedel-de Haën, ≥99.7%) was used as the model for aromatics, and *n*-heptane (H, Sigma Aldrich, 99%) and methylcyclohexane (M, Fluka, ≥99.5%) were used as models for straight, branched, and cyclic aliphatic fractions of gasoline. The T/H/M molar ratio of the prepared C_7-mixture was 20/30/50. The optimized H_2O/C and O_2/C molar ratios of the ATR feed were 3 mol/mol and 0.34 mol/mol, respectively [10].

The tubular quartz reactor (inner diameter 10 mm) was packed with 0.2 g of the catalyst and was placed in a three-zone furnace equipped with a temperature controller (Carbolite). The height of the catalyst bed was 3 mm. A pressure test for the reactor was performed with Ar (Aga, 99.999%). Subsequently, the pressure was released and the reactor was heated to 700 °C in Ar atmosphere. The C_7-mixture (0.051 ml/min(l)) and distilled water (0.149 ml/min(l)) were fed into separate evaporators (300 °C) by high performance liquid chromatography (HPLC-pumps, Agilent Technologies) equipped with micro vacuum degassers (Agilent Technologies). The vaporized feed was mixed with synthetic air (20% O_2/N_2, Aga, 99.99%) before its introduction to the reactor. The total flow rate of reactants was 300 cm^3/min (NTP) and the feed was diluted with Ar before the reactor to a total flow of 900 cm^3/min (NTP). The catalyst bed temperature and the temperature profile of the reactor were followed with a thermocouple placed inside the reactor.

For comparative purpose, ATR experiments were performed on pure ZrO_2 (0.2 g) and without any catalyst (empty reactor). The temperature range examined was 400–900 °C. The stability of the catalysts was studied at 700 °C for 5–6 h. After the experiment, the reactor was flushed with Ar and cooled down to room temperature. The amount of carbon in the fresh and used catalyst samples was determined with a Leco SC-444, where the carbon was burnt from the sample in O_2 at 1350 °C. The analytical error of the procedure was ±5%.

2.4. Product analysis and calculations

After the reactor, the flows were diluted with N_2 (900 cm^3/min, NTP) and analyzed using an on-line Fourier transform infrared (FTIR) spectrometer (Gasmet™) equipped with a Peltier-cooled mercury-cadmium-telluride (MCT) detector and multicomponent analysis software (Calcmet). The sample cell was kept at 230 °C to avoid condensation of the fed hydrocarbons and water. The compounds analyzed were H_2O, CO, CO_2, CH_4, C_2H_2, C_2–C_5 alkenes, C_2–C_7 alkanes, C_1–C_4 alcohols, benzene, toluene, cyclohexane, and methylcyclohexane. After the FTIR analysis, water and higher hydrocarbons were condensed and the dry gas flow rate was measured. The measured values were used to determine the element balances (C, H, and O) and to calculate the amounts of H_2 formed and O_2 consumed. The conversions of toluene, *n*-heptane, methylcyclohexane, and water were calculated from the feed and product flows. The weighted average of the conversions of toluene, *n*-heptane, and methylcyclohexane was calculated to present the overall hydrocarbon conversion:

$$X = 0.2X_T + 0.3X_H + 0.5X_M \quad (7)$$

The unreacted reactants and the inert gases (Ar + N_2) were excluded from the product distribution calculations (P_i (mol%), Eq. (8)), where F_i is the molar flow (mol/min) of compound *i*.

$$P_i = \frac{F_i}{\sum_{n=1}^{j} F_n} \times 100\%, \quad (8)$$

The yield of compound *i* was defined as the molar ratio of compound *i* to the total mole amount of carbon in the C_7-hydrocarbon feed (mol/mol C_{in}):

$$Y_i = \frac{F_i}{F_{C_{in}}} = \frac{F_i}{7 \cdot F_{in}(C_7\text{-mixture})} \quad (9)$$

The catalyst selectivity for reforming reactions is presented as the reforming to oxidation molar ratio (Ref/Ox, Eq. (10)). H_2 is formed not only in the reforming reactions but also by the WGS equilibrium reaction (Eq. (6)), thus the production of H_2 does not directly reveal the catalyst selectivity for reforming. However, when considering the Ref/Ox molar ratio, the effect of the WGS reaction is eliminated [15].

$$\text{Ref/Ox} = \frac{F(H_2) + F(CO)}{F(H_2O) + F(CO_2)} \quad (10)$$

Thermodynamic calculations for ATR reactions of the C_7-mixture were performed with HSC Chemistry version 5.11 [29]. The effect of side reactions such as the WGS (Eq. (6)), thermal cracking, and carbon formation reactions (Eqs. (2)–(4)) was included. Also hydrogenation and dehydrocyclization reactions of the C_7-hydrocarbons were studied.

3. Results

3.1. Catalyst characterization

The synergism between Rh and Pt on the bimetallic catalysts was examined with several characterization methods. Also the influence of calcinations temperature on catalytic properties was investigated.

3.1.1. Metal loadings

Metal loadings of the fresh (calcined) and used noble metal catalysts are shown in Table 1. There was a good correspondence between the ICP-AES and XRF results for the bimetallic RhPt catalysts. However, for the monometallic Rh catalysts, the metal loading determination by ICP-AES gave clearly lower values than was intended (0.5–1.0 wt%) or determined with XRF (Table 1). The lower Rh concentration obtained with ICP-AES indicated that the Rh from the monometallic catalysts did not completely dissolve in the acid solution used in the determination. This is in agreement with the results reported by Danzaki and Ashino [30]. In the presence of Pt, however, the solubility of Rh improved (Table 1). The calcination temperature (700 and 900 °C) did not affect the metal loading.

3.1.2. Physisorption, chemisorption, and DRITFS measurements

The measured BET-surface areas (m^2/g), total pore volumes (cm^3/g), and irreversible H_2 chemisorption uptakes of the fresh catalysts are presented in Table 2. As expected, the BET-surface area of the ZrO_2 support decreased with increasing calcination temperature (600–900 °C) [12]. A decrease in the BET-surface area, the total pore volume, and the irreversible H_2 chemisorption was also measured on catalysts calcined at 900 °C in contrast to catalysts calcined at 700 °C, indicating a change in the surface structure. The BET-surface area and the pore volume were not affect by the Rh/(Rh + Pt) molar ratio (Table 2), however, neither were the CO adsorption states of the monometallic Rh catalyst [15] affected when Rh was combined with Pt in the bimetallic 2RhPt catalyst (DRIFTS results not presented). Nonetheless, the irreversible H_2 chemisorption uptakes of the bimetallic 1RhPt and 2RhPt catalysts were superior to those of the monometallic catalysts (Table 2).

Table 1
Metal loadings of the ZrO_2-supported mono- and bimetallic RhPt catalysts calcined at 700 and 900 °C

	Metal loading (wt%) (intended)		T_{calc} (°C)	Metal loading (ICP-AES) (wt%) (fresh)			Molar ratios (mol/mol)		Metal loading (XRF) (wt%) (fresh)			Molar ratios (mol/mol)		Metal loading (ICP-AES) (wt%) (used)		
	Rh	Pt		Rh	Pt	M_{tot}[b]	Rh/Pt	Rh/(Rh + Pt)	Rh	Pt	M_{tot}[b]	Rh/Pt	Rh/(Rh + Pt)	Rh	Pt	M_{tot}[b]
Pt	–	0.50	700[a]	–	0.45	0.45	–	0.00	–	0.45	0.45	–	0.00	–	0.44	0.44
			900	–	0.39	0.39	–	0.00	–	n.a.	n.a.	–	0.00	–	0.38	0.38
0.5RhPt	0.10	0.40	700	0.05	0.33	0.38	0.29	0.22	n.a.	n.a.	n.a.	–	–	0.09	0.36	0.45
			900	0.13	0.34	0.47	0.72	0.42	0.15	0.37	0.52	0.8	0.43	0.12	0.34	0.46
1RhPt	0.17	0.33	700[a]	0.16	0.26	0.42	1.2	0.54	0.18	0.29	0.47	1.2	0.54	0.12	0.28	0.40
			900	0.16	0.25	0.41	1.2	0.55	0.19	0.25	0.44	1.4	0.59	0.16	0.25	0.41
2RhPt	0.26	0.24	700[a]	0.21	0.16	0.37	2.4	0.71	0.24	0.22	0.46	2.4	0.67	0.17	0.21	0.38
			900	0.20	0.14	0.34	2.7	0.73	0.25	0.22	0.47	2.2	0.68	0.26	0.17	0.43
Rh	0.50	–	700[a]	0.22	–	0.22		1.0	0.49	–	0.49	–	1.0	0.29		0.29
			900[a]	0.24	–	0.24	–	1.0	n.a.	–	n.a.	–	–	0.25	–	0.25
Rh	1.00	–	700	0.26	–	0.26	–	1.0	0.92	–	0.92	–	1.0	n.a.	–	n.a.

n.a.: not available.
[a] The metal loadings of fresh catalysts determined by ICP-AES are reported by Kaila et al. [15].
[b] M: metal, M_{tot} = m(Rh) + m(Pt).

Table 2
Physisorption and chemisorption results on ZrO_2-supported mono- and bimetallic RhPt catalysts calcined at 700 and 900 °C

Catalyst	T_{calc} (°C)	t_{calc} (h)	BET (m^2/g_{cat})	Total pore volume above 10 Å (cm^3/g_{cat})	Irreversible chemisorption of H_2 ($\mu mol/g_{cat}$)
ZrO_2	600	16	47	0.21	n.a.
	700	16	35	0.20	n.a.
	800	16	26	0.17	n.a.
	900[a]	16[a]	20	0.19	1.5[b]
Pt	700	1	17	0.15	0.13[b]
	900	1	18	0.094	0.01
0.5RhPt	700	1	21	n.a.	1.8
	900	1	18	0.094	n.a.
1RhPt	700	1	20	0.096	4.5
	900	1	14	0.090	0.05
2RhPt	700	1	23	0.092	4.3
	900	1	17	0.089	1.4
Rh	700	1	20	0.096	3.1[b]
	900	1	19	0.093	1.3

The intended total metal loading of the catalysts was 0.5 wt%. n.a.: not available.
[a] Calcination temperature and time used for the support of the noble metal catalysts.
[b] The H_2 chemisorption uptakes are reported by Kaila et al. [15].

3.1.3. H_2-TPR

H_2-TPR measurements were performed on fresh Rh(700), Pt(700), 2RhPt(700), and 2RhPt(900). On the Rh(700) catalyst, two reduction steps, at 95 and 127 °C (Fig. 1), were detected. Similar reduction steps were also found in a study on aged Rh catalysts supported on various materials published by Ferrandon and Krause [31]. On Pt(700), no indication of reducible species was observed, which agrees with the low irreversible H_2 chemisorption uptakes (Table 2) and the fact that Pt does not form stable oxides at high temperatures [17,32]. On the bimetallic 2RhPt(700) and 2RhPt(900) catalysts only one reduction step was noticed and the reduction temperature shifted with the calcination temperature (Fig. 1). Moreover, the consumption of H_2 was clearly lower with these bimetallic catalysts compared to the monometallic Rh, the $A_{2RhPt(700)}/A_{Rh}$ and $A_{2RhPt(900)}/A_{Rh}$ ratios in Fig. 1 being 16% and 25%, respectively. If it is assumed that only Rh compounds reduce and according to the H_2 consumption and the Rh-loadings determined by XRF (Table 1), only 33% and 50% of Rh atoms were in reducible form on the 2RhPt(700) and 2RhPt(900) catalysts, respectively.

3.1.4. XRD and XPS

The XRD spectra of the bimetallic catalysts showed overlapping of the Rh, Pt, and possible Rh_xPt_{1-x} alloy peaks with those corresponding to ZrO_2 making the identification of the species difficult. Subsequently, Rh and Pt peaks were identified in the XPS spectra. Some differences were noticed in the intensities of the Rh and Pt peaks on the mono- and bimetallic catalysts. However, the metal loadings were too low for reliable characterization.

3.1.5. SEM

SEM was used to examine the surface morphology of fresh and used Rh(700), Rh(900), Pt(700), Pt(900), 2RhPt(700), and 2RhPt(900) catalysts. No metal clusters were detected on the surface of fresh Rh(700) and Rh(900) catalysts (data not presented). Thus, either the impregnation procedure was successful and therefore

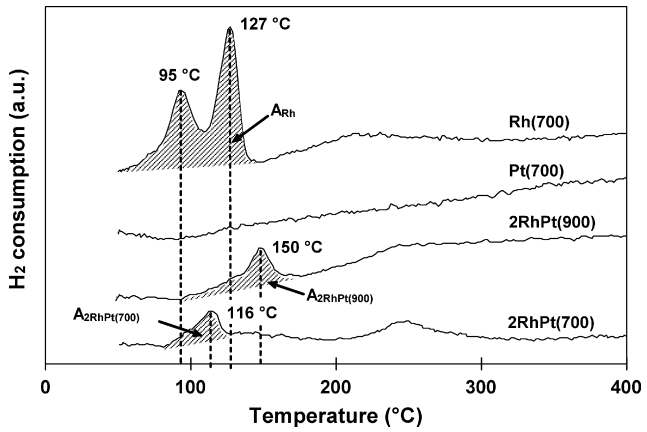

Fig. 1. H_2-TPR profiles of fresh Rh(700), Pt(700), 2RhPt(900), and 2RhPt(700) catalysts. A = area of the H_2 consumption peak.

well-dispersed metal particles were obtained, or the Rh particles were encapsulated within the ZrO_2 [19,20]. The SEM pictures of the Pt(700), Pt(900), 2RhPt(700), and 2RhPt(900) catalysts showed dispersed metal particles on the surface of the fresh catalysts (Fig. 2). On the 2RhPt(700) and 2RhPt(900) catalysts, moreover, an orthorhombic crystal structure of the metal particles was perceived (Fig. 2b).

3.1.6. EDX

EDX measurements were performed on the fresh 2RhPt(900) catalyst. EDX spectra were measured on several metal particles and on the surface of the ZrO_2 support. The metal particles of different sizes contained Rh and Pt with an average Rh/Pt ratio of 0.10 mol/mol; the variation being 0.03–0.19 mol/mol for 34 particles. Moreover, within single particles the variation in Rh/Pt ratio was small (e.g. 0.10–0.14 mol/mol) indicating homogenous distribution of Rh and Pt metals. The Rh/Pt ratio (0.10 mol/mol) of the 2RhPt(900) catalyst surface ($d < 0.5$–1.5 μm) was clearly lower than the Rh/Pt ratio measured for the whole catalyst (2.2–2.7 mol/mol) (Table 1), the catalyst being strongly Rh-depleted. Nonetheless, Rh or Pt was not found in the support ($d < 0.5$–1.5 μm).

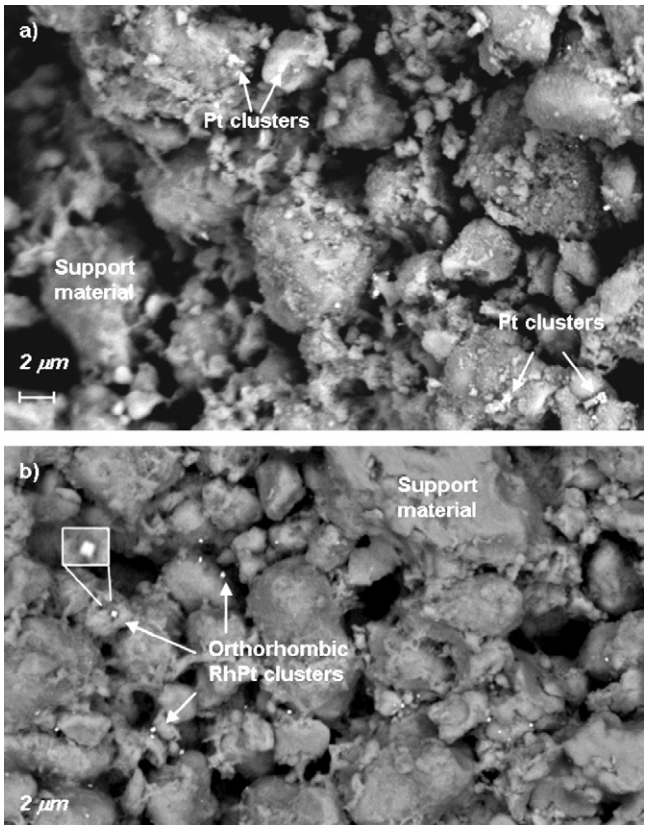

Fig. 2. SEM pictures of fresh (a) Pt(900) and (b) 2RhPt(900) catalysts.

3.2. Catalyst testing in ATR of simulated gasoline

The mono- and bimetallic RhPt catalysts were tested in ATR of simulated gasoline at temperatures between 400 and 900 °C to get insight on the effect of Rh/(Rh + Pt) molar ratio on catalyst performance. Also the effect of calcination temperature (700 and 900 °C) on catalyst performance was evaluated. Short-term stability tests were performed at 700 °C for 5–6 h, and the carbon deposition and metal loadings of the used catalysts were determined. The catalyst sintering was examined with SEM after testing.

3.2.1. Non-catalytic experiments

The involvement of non-catalytic reactions of the simulated gasoline was investigated at ATR conditions in an empty reactor and the results are shown in Fig. 3. At low inlet temperatures (400–500 °C), the thermal cracking of simulated gasoline was negligible. The conversions of *n*-heptane, methylcyclohexane, and oxygen increased with temperature, and complete decomposition of aliphatic hydrocarbons was reached at the inlet temperature of 750 °C. This is in agreement with thermal cracking experiments of the individual hydrocarbons reported in our earlier study [10]. In the temperature range 500–700 °C dehydrocyclization of *n*-heptane or the reaction of methylcyclohexane to toluene and H_2 took place, in agreement with thermodynamic calculations. The formation of toluene was highest at 700 °C (Fig. 3). Beyond 700 °C toluene started to react and at 900 °C almost complete decomposition was obtained (Fig. 3). The product distribution at 700 °C is included in Table 3. The negative value obtained for the water conversion at 700–900 °C and the sharp increase in oxygen consumption (Fig. 3) indicated formation of water by complete oxidation (OX) reactions.

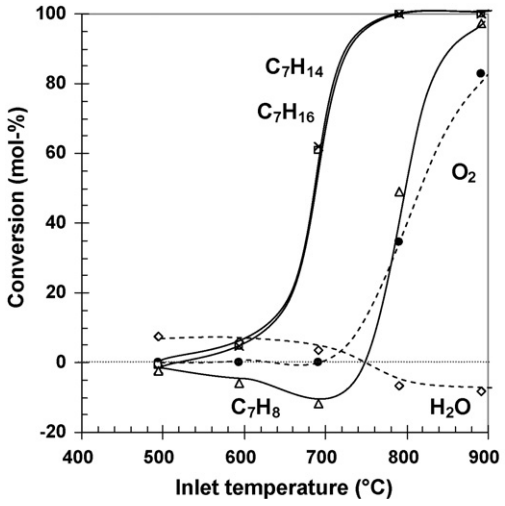

Fig. 3. Conversions (C_7H_{16} (×), C_7H_{14} (□), C_7H_8 (△), H_2O (◇), and O_2 (●)) in non-catalytic experiments of the simulated gasoline in ATR conditions (H_2O/C = 3 mol/mol, O_2/C = 0.34 mol/mol).

Table 3
Product distribution (mol%) in ATR of simulated gasoline at the inlet temperature of 700 °C

	Conversion (mol%)		Distribution of products (mol%)[a]				
	C7-mixture	Water	H_2	CO	CO_2	CH_4	Others
Thermodynamics	100	25	67	11	23	0	0
No catalyst	47	4.8	61	9.0	0.2	4.9	25
ZrO_2	51	−5.7	27	53	14	3.6	2.1
Pt(900)	53	4.9	50	29	17	0.9	3.1
0.5RhPt(900)	98	27	61	17	21	0.2	0.2
1RhPt(900)	97	29	62	18	20	0.4	0.5
2RhPt(900)	99	27	63	17	19	0.3	0.2
Rh(900)	97	29	59	17	22	0.3	0.6

The intended total metal loading of the mono- and bimetallic catalysts was 0.5 wt%.
[a] Reactants are excluded from the calculation.

3.2.2. Comparison of mono- and bimetallic RhPt catalysts

The hydrocarbon and water conversions in ATR of simulated gasoline on the mono- and bimetallic RhPt catalysts are presented in Fig. 4a and b, respectively. The conversions obtained with the bimetallic catalysts were between the conversions obtained with monometallic Rh and Pt. As expected [15], the conversion of water was highest on Rh, and the maximum value was reached at 700 °C.

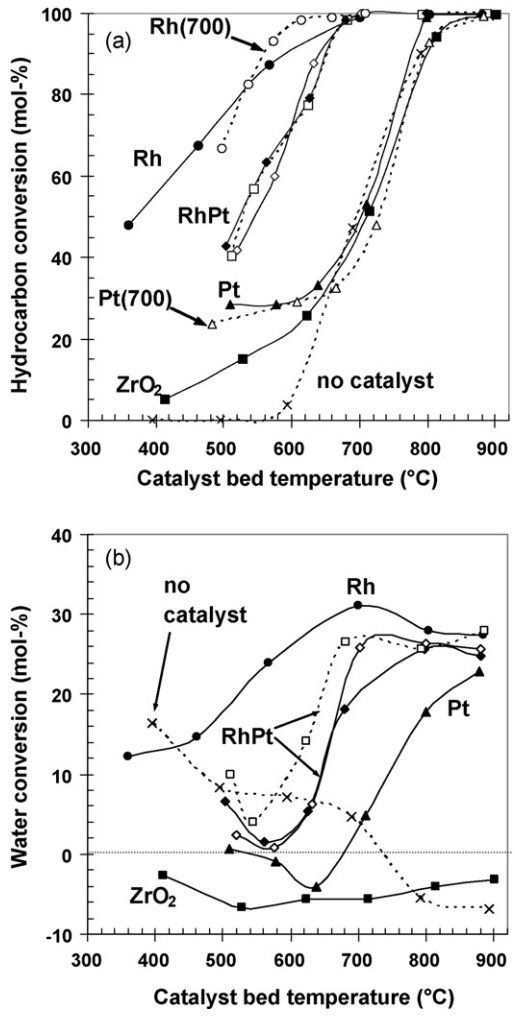

Fig. 4. (a) The overall hydrocarbon conversion and (b) the conversion of water in ATR of simulated gasoline on Rh(900) (●), Rh(700) (○), 2RhPt(900) (◆), 1RhPt(900) (◇), 0.5RhPt(900) (□), Pt(900) (▲), Pt(700) (△), ZrO_2 (■), and without any catalyst (×). H_2O/C = 3 mol/mol, O_2/C = 0.34 mol/mol.

At 700 °C, moreover, complete hydrocarbon conversions were obtained on all the Rh-containing mono- and bimetallic catalysts (Fig. 4a), whereas the activity of Pt was low. Thus, only a small addition of Rh was sufficient to improve the performance of bimetallic catalysts over that of monometallic Pt. The Rh/Pt ratio of the bimetallic catalysts had no effect on the catalyst activity, as the hydrocarbon conversion was equal on all the bimetallic catalysts calcined at 900 °C (Fig. 4a). On catalysts calcined at 700 °C, slight differences in the catalyst activities were noticed (data not reported). Thus, the higher calcination temperature equalized the bimetallic RhPt catalysts.

On all noble metal catalysts, the conversion of oxygen was complete in the entire temperature range tested (inlet temperature 400–900 °C), revealing activity for oxidation reactions (i.e. POX and OX), whereas on the support the consumption of oxygen increased with temperature and complete conversion was reached at 850 °C.

Table 3 compares the product distributions obtained on the mono- and bimetallic RhPt catalysts in ATR of simulated gasoline at inlet temperature of 700 °C. For comparative purpose, also the thermodynamic equilibrium of the products and results on ZrO_2 and in non-catalytic experiments are presented. Although the pure support does not catalyze the reforming reactions [15] the selectivity for CO_x (Table 3) improved on ZrO_2 when compared to non-catalytic experiments, revealing some catalytic behavior. Indeed, oxidation reactions were taking place on ZrO_2 as water was formed more than consumed. The presence of Pt increased the H_2 production, but thermal cracking products were still formed, correlating with the low reforming activity. On all Rh-containing mono- and bimetallic catalysts, the product distribution was close to the thermodynamic equilibrium. Moreover, the low concentrations of light hydrocarbons (C_1–C_4-hydrocarbons designated as "others" in Table 3) indicated the limited extent of thermal cracking reactions and high reforming activity for all Rh-containing catalysts [10].

The WGS reaction (Eq. (6)) clearly affected the product distribution on Rh-containing catalysts, as is observed, e.g. from the product yields obtained on 2RhPt(900) (Fig. 5), whereas on Pt the conversion of H_2O and CO to H_2 and CO_2 remained lower (Table 3). The contribution of WGS was neglected in the Ref/Ox ratio (Eq. (10)), which is presented in Fig. 6 as the function of intended Rh/(Rh + Pt) molar ratio of the mono- and bimetallic catalysts. The Ref/Ox ratio was highest on 2RhPt and lowest on Pt.

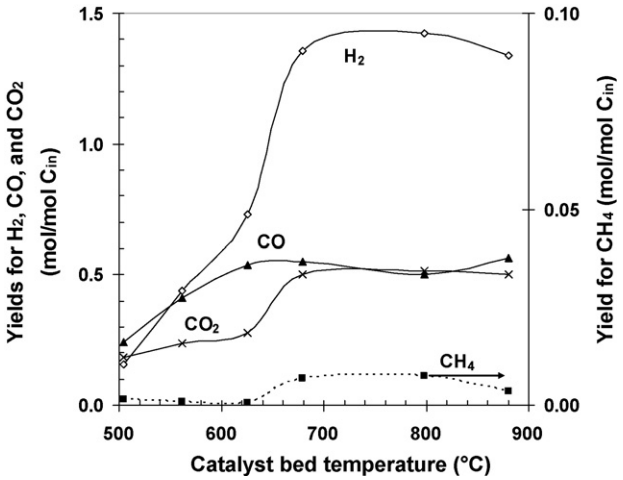

Fig. 5. Yields (mol/mol C_{in}) for H_2 (◇), CO (▲), CO_2 (×), and CH_4 (■) in ATR of simulated gasoline on the 2RhPt(900) catalyst. H_2O/C = 3 mol/mol, O_2/C = 0.34 mol/mol.

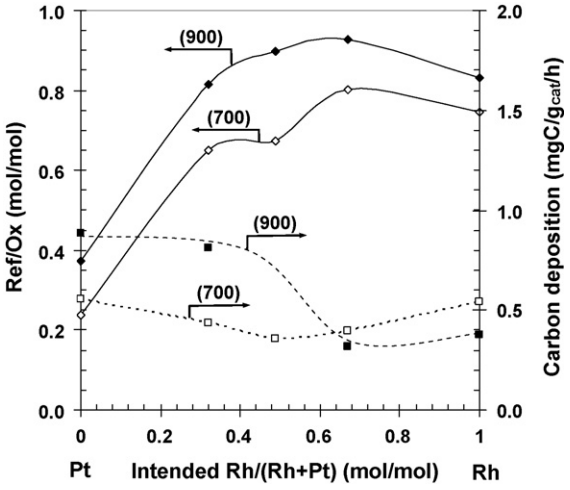

Fig. 6. Effect of the Rh/(Rh + Pt) molar ratio on the Ref/Ox ratio (◆) (mol/mol) of the products and on the average carbon deposition (■) (mgC/g_{cat}/h) in ATR of simulated gasoline on mono- and bimetallic RhPt catalysts (0.2 g) calcined at 700 °C (open symbol) and 900 °C (filled symbol). H_2O/C = 3 mol/mol, O_2/C = 0.34 mol/mol, 700 °C for 5–6 h.

Both, the activity for OX and the presence of thermal cracking, decreased the reforming selectivity of Pt.

3.2.3. Short-term stability of RhPt catalysts

The stability of RhPt catalysts, calcined at 700 or 900 °C, was studied at 700 °C for 5 or 6 h, respectively. The H_2 production is presented in Fig. 7 for catalysts calcined at 700 °C. The H_2 production decreased with time on Rh(700) and 0.5RhPt(700) indicating a change in the catalyst structure or even catalyst deactivation, as was expected for Rh [10,15]. Also the decrease in conversions and the increase in thermal cracking products, mainly ethene, reflected the deactivation of Rh(700). On 0.5RhPt(700), on the other hand, neither a decrease in the hydrocarbon conversions was observed nor thermal cracking products were formed, revealing improved stability compared to that of Rh(700). The stability of the bimetallic RhPt catalysts improved further with the increase in Rh/Pt ratio (Fig. 7). Also the higher calcination temperature (900 °C) stabilized the surface structure of the mono- and bimetallic RhPt catalysts, as the product distribution and the conversions remained constant during the whole experiment (data not reported).

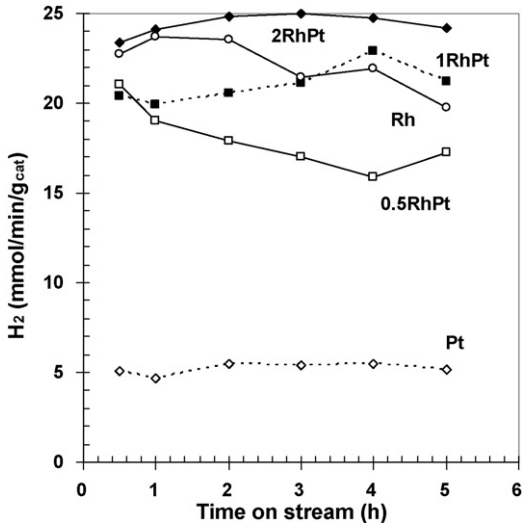

Fig. 7. Formation of H_2 (mmol/min/g_{cat}) as a function of time in ATR of simulated gasoline (700 °C/5 h) on Pt(700) (◇), 0.5RhPt(700) (□), 1RhPt(700) (■), 2RhPt(700) (◆), and Rh(700) (○) catalysts (0.2 g). H_2O/C = 3 mol/mol, O_2/C = 0.34 mol/mol.

Under the conditions of the stability test (700 °C), the reforming activity and selectivity of monometallic Pt catalysts were low. Nonetheless, the Pt(700) catalyst remained stable (Fig. 7). In fact, the hydrocarbon and water conversions improved with time. Similar results on Rh deactivation and Pt stability were reported for SR of biomass-derived pyrolysis oil [33]. According to Bitter et al. [32], the activity of a Pt catalyst is linearly proportional to the concentration of the Pt-ZrO_2 interface, whereas the activity of Rh catalysts is directly proportional to the availability of Rh. Hence, Rh catalysts are more sensitive for deactivation.

3.2.4. Carbon deposition

After the stability tests (700 °C/5–6 h), carbon deposition (Fig. 6) of the used catalysts was measured. On all catalysts, the carbon deposition was extremely low, as less than 0.01 mol% of the fed carbon (2.9 mmol C/min) was accumulated on the catalysts. On bimetallic catalysts, moreover, the carbon deposition was lower than on monometallic catalysts, which is especially evident for the calcination temperature of 700 °C. The average carbon deposition (Fig. 6) was highest on the monometallic Pt catalyst (0.55–0.88 mg/g_{cat}/h), as was proposed owing to the high amounts of thermal cracking products formed. Indeed, alkenes, in particular ethene, are considered carbon precursors [34]. Moreover, the average carbon deposition per hour corresponded to that reported by Souza and Schmal [14] for Pt/ZrO_2 catalyst tested in dry reforming of methane (0.8–0.9 mg coke/g_{cat}/h). Despite of the carbon deposition (Fig. 6) and the presence of thermal cracking, no deactivation nor changes in the product distribution of the Pt(700) or Pt(900) catalysts were observed with time.

On the monometallic Rh catalysts, the carbon deposition (0.37–0.54 mg/g_{cat}/h) was lower than on Pt, in agreement with the results of Cavallaro et al. [35]. They suggested that only small amounts of whisker carbon are formed in ATR on Rh/Al_2O_3 catalysts, and this type of carbon easily reacts with oxygen regenerating the surface [35]. The same conclusions on the effect of oxygen were drawn in SR studies of biomass-derived pyrolysis oil, where a higher amount of carbon was deposited on Rh/$Ce_{0.5}Zr_{0.5}O_2$ than on Pt/$Ce_{0.5}Zr_{0.5}O_2$, but this carbon was mostly burnt off during regeneration [33]. Although carbon is easily burnt off with O_2 (present in ATR) the Rh(700) catalyst deactivated with time (Fig. 7).

When the deposited carbon is removed by CO_2 (Eq. (3)) or H_2O (Eq. (4)), additional H_2 and CO are formed. Hence, the high amount of CO along with the lower amount of CO_2 on Pt and ZrO_2 (Table 3) reveal the presence of reverse-Boudouard reaction (Eq. (3)) at 700 °C, as favored by thermodynamics. This observation is, furthermore, in good agreement with CO_2 pulsing experiments performed by Bitter et al. [32] on coked Pt/ZrO_2. They suggested that the ability of the ZrO_2 support to release oxygen might be important in CO formation [32].

With elevated calcination temperature (900 °C), carbon deposition increased on catalysts with higher Pt loading, and decreased on catalysts with higher Rh-loading. With both calcination temperatures, lowest amounts of deposited carbon were measured on 2RhPt catalysts. The results on carbon deposition agreed with those on catalyst activity, selectivity, and stability, as carbon deposition was lowest on catalysts, where the H_2 formation was stable (Fig. 7) and the Ref/Ox ratio was highest (Fig. 6).

3.2.5. Characterization of used catalysts

Metal loadings of the used catalysts were determined (Table 1). Slight differences were detected in the metal loadings of the fresh and used catalysts. These differences are explained by the

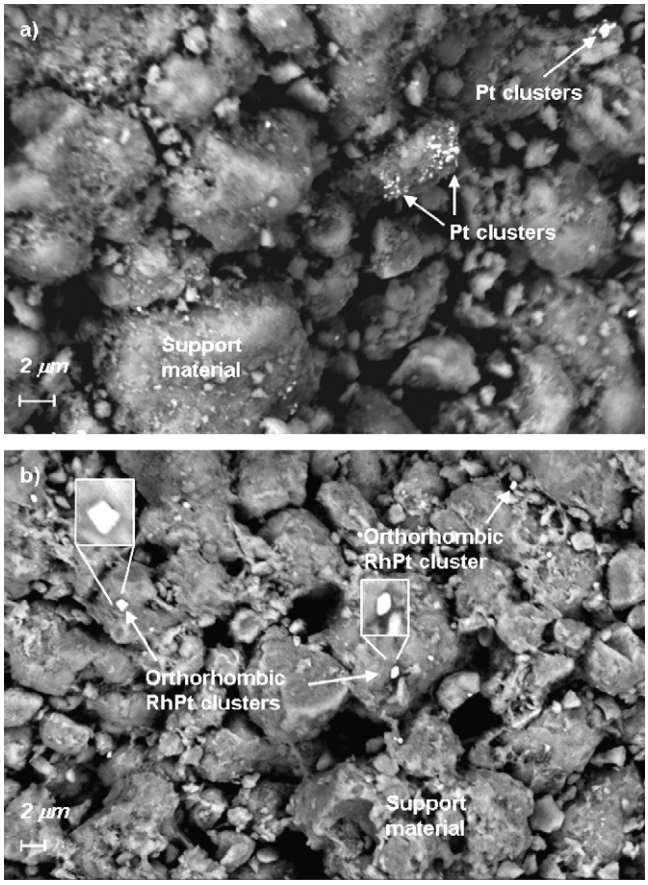

Fig. 8. SEM pictures of used (a) Pt(900) and (b) 2RhPt(900) catalysts. Catalysts were tested in ATR of simulated gasoline (H_2O/C = 3 mol/mol, O_2/C = 0.34 mol/mol).

analytical error of ICP-AES [30] and the difficulties in dissolution of Rh into the acid, not excluding the possibility of moisture present in the fresh sample. In contrast to our earlier results [15], no depletion of Rh was perceived after the stability tests (700 °C).

In SEM measurements, no sintering of Rh was observed, as only the support structure was visible on the used Rh(700) and Rh(900) catalysts. On Pt-containing catalysts, that is Pt(700), Pt(900), 2RhPt(700), and 2RhPt(900), however, significant sintering was noticed. Furthermore, on the monometallic Pt catalysts (Fig. 8a), large metal clusters of undefined shape were detected, whereas on the used 2RhPt catalysts (Fig. 8b), the large metal clusters had clearly an orthorhombic structure.

4. Discussion

4.1. Catalytic performance of bimetallic RhPt catalysts

The catalytic performance of an average alloy is better than that of the less active metal (Pt) but lower than that of the most active metal (Rh) [25]. However, if there is synergism between the two metals, the performance of the alloy is even better than that of the more active metal [24–26]. Summarizing the results on catalyst performance, synergism between Rh and Pt is evident on the ZrO_2-supported bimetallic catalysts. On catalysts where Rh predominated, improved catalyst selectivity (Ref/Ox, Fig. 6) and stability (Fig. 7) were obtained. Hence, a slight addition of Pt improved the Rh catalyst selectivity and stability markedly and increased the H_2 chemisorption uptake (Table 2). Respectively, only a slight addition of Rh was sufficient to improve the catalyst activity of the bimetallic catalyst over that of the monometallic Pt (Fig. 4).

On Pt-containing catalysts, however, strong sintering was observed during aging in ATR (Fig. 8), which is fully inconsistent with the high activity and stability observed, i.e. for the bimetallic 2RhPt catalysts. Indeed, Pt is more sensitive to sintering than Rh owing to its lower melting point and the migration sensitivity [22,36]. Besides, due to the low surface area of ZrO_2 (Table 2), the surface concentrations of the noble metals (0.5 wt%) are relatively high, which promotes sintering. For monometallic Rh and Pt catalysts, the calculated surface concentrations are 2.4 μmol Rh/m^2 and 1.2 μmol Pt/m^2, respectively. Furthermore, as sintering accelerates with temperature, the metal particle size on 2RhPt(900) is larger than on 2RhPt(700), thus requiring higher temperatures for reduction (Fig. 1).

4.2. Presence of a Rh_xPt_{1-x}–Rh_2O_3 equilibrium

Recently, Kolb et al. [37] claimed that the binary alloys of Rh, Pd, Ir, and Pt were misunderstood for nearly half a century and there exists no immiscibility in the Rh_xPt_{1-x} system below 760 °C [38], which was also disproved by Jacob et al. [39] in thermodynamic measurements. Besides, Jacob et al. introduced the presence of an alloy-oxide equilibrium in the Rh-Pt-O ternary system measured on an Y_2O_3-stabilized ZrO_2 solid electrolyte [17,39]. Considering the miscibility of the Rh_xPt_{1-x} system, the presence of an alloy on the bimetallic catalysts is possible with all Rh/Pt ratios. Moreover, in an oxidizing environment the formation of equilibrium between the Rh_xPt_{1-x} alloy and Rh_2O_3 is possible [17].

It is presented that Rh_xPt_{1-x} alloys result in a strong Pt enrichment of the surface as the temperature increases (maximum at 830 °C) [23,40], which agrees with our results on the composition (EDX) of the metal particles of 2RhPt(900). Furthermore, an ordered Rh oxide overlayer is formed on such Pt-enriched bimetallic surfaces (e.g. Rh/Pt(100) and Pt/Rh(100)) [41]. Indeed, Rh_xPt_{1-x} alloys have been classified as near-surface alloys (NSAs) owing to the tendency of subsurface metal layer formation [42].

In SEM measurements, orthorhombic metal clusters were detected on the fresh (Fig. 2b) and used (Fig. 8b) bimetallic catalysts. These orthorhombic crystals differ from the lattice structure proposed for pure Rh or Pt crystals (face-centered cubic (fcc) crystals (Pearson's symbol cF4)) [43], or the cubo-octahedral shape predicted for the Rh_xPt_{1-x} alloy clusters [44]. After high temperature (>500 °C) oxidation treatments, however, a stable, orthorhombic structure for Rh_2O_3 is confirmed [45]. Moreover, reducible Rh species similar to Rh_2O_3 are reported to be the active form of Rh [46], which would explain the high catalytic performance of these bimetallic catalysts. Both metals (Rh and Pt) were found in all metal particles of the 2RhPt(900) catalyst (EDX), which supports our suggestion of a Rh_xPt_{1-x} alloy that is incased in the core of the Rh_2O_3 layer. On monometallic Pt catalyst neither reducible species (TPR, Fig. 1) nor orthorhombic crystals (SEM, Fig. 2) were detected, consistent with the low reforming activity.

According to the TPR-, SEM-, and EDX-results and when considering the improved catalyst performance, we suggest the presence of the Rh-Pt-O ternary system on the bimetallic RhPt/ZrO_2 catalysts, where the metal clusters consist of a Rh_xPt_{1-x} alloy subsurface and a Rh_2O_3 overlayer. A scheme for the synergism between Rh and Pt on the ZrO_2-support and the formation of Rh_xPt_{1-x}–Rh_2O_3 equilibrium under oxidizing conditions is presented in Fig. 9. On the monometallic Rh catalyst (Fig. 9a), interaction with the support is strong and continues during the aging in ATR. Moreover, the migration of various supports such as CeO_2 [19,31], TiO_2 [20], Al_2O_3 [31], and YSZ [31] on top of the Rh crystallites is possible. Therefore, the migration of the support or

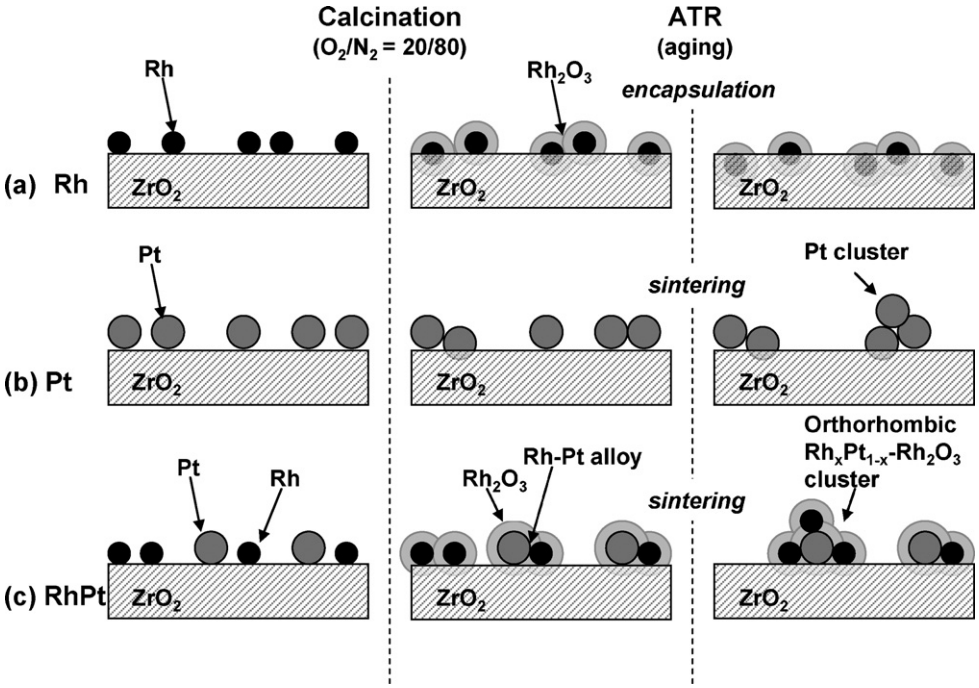

Fig. 9. A scheme for the interactions of Pt and Rh on ZrO_2-supported (a) Rh, (b) Pt, and (c) RhPt catalysts under oxidizing conditions of calcination and aging in ATR.

the migration of Rh into the support cannot be excluded in the case of ZrO_2 [47]. Owing to the possible Rh encapsulation, the Rh-loading of the catalyst is most likely concentrated into lower layers of the catalyst, thereby explaining why metal particles were not detected in the SEM measurements of the monometallic Rh catalysts. Subsurface metal layers might, still, affect the binding of adsorbed species, yielding varied reaction rates and selectivities for the catalytic process [48]. Besides, as part of the Rh is encapsulated in the support, a second reduction step at higher temperature (TPR, Fig. 1) is needed for the reduction of the Rh oxides that are in strong interaction with the support [31].

Also for Pt/ZrO_2 (Fig. 9b), strong metal support interaction (SMSI) is observed [32,47], and either the formation of a Pt-Zr alloy or the Pt encapsulation in ZrO_2 is suggested [47]. As Pt is in metallic state (Pt^0), the strong interaction with the support is, however, not noticed in the H_2-TPR (Fig. 1).

On the bimetallic catalysts (Fig. 9c), the formation of the Rh_xPt_{1-x} alloy impairs the SMSI [11]. Hence, the encapsulation of the noble metals (Rh and Pt) is prevented, and the Rh_2O_3, formed under oxidizing conditions, is reduced in one step only (Fig. 1). Owing to the Rh_xPt_{1-x}–Rh_2O_3 equilibrium part of the Rh is present in the reduced state (Rh^0), thus decreasing the consumption of H_2 during TPR (Fig. 1).

The Rh_2O_3 is the active site of the mono- (Rh) and bimetallic (RhPt) catalysts, but the strong interaction of Rh with the ZrO_2-support and the possible encapsulation of Rh deactivate the three-way catalyst (Rh/Ce-ZrO_2) with time [46]. According to the presented results, a slight addition of Pt is, however, sufficient to improve the catalyst performance of Rh in ATR of simulated gasoline. Due to the synergism of Rh and Pt, a Rh_xPt_{1-x} alloy is formed, which impairs the interaction of the metals with the support [11], as is demonstrated in Fig. 9. Moreover, the amount of active Rh_2O_3 can be controlled with the Rh/Pt ratio [17,49], temperature, and partial pressure of O_2 that together affect the Rh_xPt_{1-x}–Rh_2O_3 equilibrium in the Rh-Pt-O ternary system [17].

5. Conclusions

ATR of simulated gasoline was studied on ZrO_2-supported mono- and bimetallic RhPt catalysts. Only a small addition of Rh improved the activity of the Pt catalyst markedly. In selectivity and stability the bimetallic RhPt catalysts were superior to the monometallic Rh or Pt catalysts. The reforming activity of the bimetallic catalysts was intermediate between those of the monometallic Rh and Pt catalysts, in proportion to the Rh-loading.

At high calcination temperature, the BET-surface area and the irreversible H_2 chemisorption uptakes decreased and sintering of the catalysts was detected. Still, the higher calcination temperature had a stabilizing effect on all the catalysts and improved the selectivity for reforming. With high calcination temperature (900 °C), the carbon deposition increased when Pt predominated and decreased when Rh was predominant, likely due to the Boudouard reaction. Thus, changing the Rh/Pt ratio can optimize the RhPt catalyst performance, not forgetting the effect of calcination temperature.

Based on the TPR-, SEM-, and EDX-results and the behavior of the bimetallic catalysts in ATR, strong synergism between Rh and Pt is observed. The synergism between Rh and Pt improved the performance of the catalyst, and higher selectivity and stability towards carbon deposition were obtained on bimetallic catalysts than on monometallic Rh and Pt catalysts. This was also evidenced by the Ref/Ox ratio, the production of H_2, and the carbon deposition. Moreover, we suggest the presence of a Rh_xPt_{1-x}–Rh_2O_3 equilibrium, where the Rh_2O_3 is the active site of the catalyst.

Acknowledgments

Financial support from the Finnish Funding Agency for Technology and Innovation (Tekes) is acknowledged. Dr. Erkki Heikinheimo (Department of Materials Science and Engineering, TKK) is thanked for the SEM pictures, and Dr. Joseph Campbell, Dr. Matti Putkonen, Hannu Revitzer, and Lassi Hiltunen for the XPS,

XRD, ICP-AES, and XRF determinations, respectively. Satu Korhonen is thanked for the DRIFTS measurements, and Kati Vilonen and Arto Mäkinen are thanked for their help with the Physisorption and Chemisorption determinations. Annika Hämäläinen is thanked for carrying out part of the experimental work.

References

[1] P. Ferreira-Aparicio, M.J. Benito, Cat. Rev.-Sci. Eng. 47 (2005) 491.
[2] C. Song, Catal. Today 77 (2002) 17.
[3] J.J. Strohm, J. Zheng, C. Song, J. Catal. 238 (2006) 309.
[4] J.R. Rostrup-Nielsen, in: J.R. Anderson, M. Boudart (Eds.), Catalysis: Science and Technology, vol. 5, Springler Verlag, Berlin, Heidelberg, New York, Tokyo, 1984p. 1.
[5] S.H. Clarke, A.L. Dicks, K. Pointon, T.A. Smith, A. Swann, Catal. Today 38 (1997) 411.
[6] D.L. Trimm, Z.I. Önsan, Cat. Rev.-Sci. Eng. 43 (1–2) (2001) 31.
[7] P. Cheekatamarla, A.M. Lane, J. Power Sources 152 (2005) 256.
[8] P.K. Cheekatamarla, C.M. Finnerty, J. Power Sources 160 (2006) 490.
[9] K.P. Cheekatamarla, A.M. Lane, J. Power Sources 153 (2006) 157.
[10] R.K. Kaila, A.O.I. Krause, Int. J. Hydrogen Energy 31 (2006) 1934.
[11] S. Irusta, L.M. Cornaglia, E.A. Lombardo, J. Catal. 210 (2002) 263.
[12] R. Burch, P.K. Loader, Appl. Catal., A 143 (1996) 317.
[13] T. Yamaguchi, Catal. Today 20 (1994) 199.
[14] M.M.V.M. Souza, M. Schmal, Catal. Lett. 91 (2003) 11.
[15] R.K. Kaila, A. Gutierrez, S.T. Korhonen, A.O.I. Krause, Catal. Lett. 115 (2007) 70.
[16] P.A.J. Bagot, A. Cerezo, G.D.W. Smith, Surf. Sci. 601 (2007) 2245.
[17] K.T. Jacob, S. Priya, Y. Waseda, Bull. Mater. Sci. 21 (1998) 99.
[18] C.P. Oliver, B.V. King, D.J. O'Connor, Surf. Sci. 557 (2004) 101.
[19] S. Bernal, F.J. Botana, J.J. Calvino, G.A. Ciferdo, J.A. Pérez-Omil, J.M. Pintado, Catal. Today 23 (1995) 219.
[20] O. Ozturk, J.B. Park, S. Ma, J.S. Ratliff, J. Zhou, D.R. Mullins, D.A. Chen, Surf. Sci. 601 (2007) 3099.
[21] D.C. Cronauer, T.R. Krause, J. Salinas, A. Wagner, J. Wagner, Prepr. Pap.-Am. Chem. Soc., Div. Fuel Chem. 51 (1) (2006) 297.
[22] K. Tanaka, A. Sasahara, J. Mol. Catal. A: Chem. 155 (2000) 13.
[23] F.L. Williams, G.C. Nelson, Appl. Surf. Sci. 3 (1979) 409.
[24] Z. Hu, Chem. Commun. 7 (1996) 879.
[25] R. Polvinen, Synergistic Effect and Influence of Aging Treatment on Supported Noble Metal Catalyst, Tampere University of Technology, ISBN 952-15-1253-9, Tampere, 2004, p. 65.
[26] M.S. Tzou, K. Asakura, Y. Yamazaki, H. Kuroda, Catal. Lett. 11 (1991) 33.
[27] H. Celio, M. Trenary, H.J. Robota, J. Phys. Chem. 99 (1995) 6024.
[28] S.M.K. Airaksinen, M. Bañares, A.O.I. Krause, J. Catal. 230 (2005) 507.
[29] A. Roine, HSC Chemistry for Windows version 5.11. Outokumpu Research, 2003.
[30] Y. Danzaki, T. Ashino, Anal. Sci. 17 (2001) 1011.
[31] M. Ferrandon, T. Krause, Appl. Catal. A311 (2006) 135.
[32] J.H. Bitter, K. Seshan, J.A. Lercher, J. Catal. 176 (1998) 93.
[33] E.E. Iojoiu, M.E. Domine, T. Davidian, N. Guilhaume, C. Mirodatos, Appl. Catal., A 323 (2007) 147.
[34] F. Joensen, J. Rostrup-Nielsen, J. Power Sources 105 (2002) 195.
[35] S. Cavallaro, V. Chiodo, A. Vita, S. Freni, J. Power Sources 123 (2003) 10.
[36] P. Fornasiero, J. Kaspas, V. Sergo, M. Graziani, J. Catal. 182 (1999) 56.
[37] B. Kolb, S. Müller, D.B. Botts, G.L.W. Hart, Phys. Rev. B 74 (144206) (2006) 1.
[38] G. Schlamp, Ullmann's Encyclopedia of Industrial Chemistry, John Wiley & Sons, Inc., Last updated: 30 Aug 2007, p. 42.
[39] K.T. Jacob, S. Priya, Y. Waseda, Metall. Mater. Trans. A 29A (1998) 1545.
[40] E.L.D. Hebenstreit, W. Hebenstreit, M. Schmid, P. Varga, Surf. Sci. 441 (1999) 441.
[41] K. Tanaka, Surf. Sci. 357–358 (1996) 721.
[42] J. Greeley, M. Mavrikakis, Nat. Mater. 3 (2004) 810.
[43] N.W. Ashcroft, N.D. Mermin, in: D.G. Crane (Ed.), Solid State Physics, Holt, Rinehart and Winston, Philadelphia, 1976, p. 70.
[44] L. Zhu, R. Wang, T.S. King, A.E. DePristo, J. Catal. 167 (1997) 408.
[45] D.D. Beck, T.W. Capehart, C. Wong, D.N. Belton, J. Catal. 144 (1993) 311.
[46] A. Suopanki, R. Polvinen, M. Valden, M. Härkönen, Catal. Today 100 (2005) 327.
[47] D.L. Hoang, H. Leiske, Catal. Lett. 27 (1994) 33.
[48] S. Zhou, B. Varughese, B. Eichhorn, G. Jackson, K. McIlwrath, Angew. Chem. Int. Ed. 44 (2005) 4539.
[49] F. Cimini, R. Prins, J. Phys. IV 7 (1997) 925.